INTERNATIONAL JOURNAL OF PRECISION ENGINEERING AND MANUFACTURING Vol. 16, No. 8, pp. 1771-1777 JULY 2015 / 1771
DOI: 10.1007/s12541-015-0232-9 ISSN 2234-7593 (Print) / ISSN 2005-4602 (Online)

Frequency-Dependent Nonlinear Dynamic Stiffness of Aerostatic Bearings Subjected to External Perturbations

Puliang Yu[1], Xuedong Chen[1], Xiaoli Wang[1], and Wei Jiang[1,#]

1 State Key Laboratory of Digital Manufacturing Equipment and Technology, Huazhong University of Science and Technology, Wuhan, 430074, China
Corresponding Author / E-mail: jiangw@hust.edu.cn, TEL: +86-13995632257, FAX: +86-2787559893

KEYWORDS: Aerostatic bearing, Dynamic stiffness, Perturbation, Frequency

The dynamic characteristics of aerostatic bearings are critical to the performances of ultra-precision manufacturing equipment. Dynamic characteristics have recently been recognized to be significant to the dynamic stiffness of aerostatic bearings, and related research has seldom been reported up till now. In this paper, numerical simulations and experiments are carried out to investigate the influence of perturbations on the dynamic stiffness of aerostatic bearings. The thrust bearings of an aerostatic bearing spindle are selected for simulations and experiments, while the journal bearing is used as frictionless guide way. Dynamic mesh method is adopted to simulate the variation of gas film, and numerical simulations are performed by using ANSYS-Fluent-software based on the perturbation theory. Perturbations are generated via voice coil motor under different conditions in experiments. Simulations and experimental results reveal that the dynamic stiffness is much more sensitive to the perturbation frequency rather than the nanoscale perturbation amplitude. For the same amplitude of displacement perturbations, the axial stiffness coefficient increases whereas the axial damping coefficient decreases with the increase of perturbation frequency. It indicates that the dynamic stiffness of aerostatic bearings can be significantly improved by using active control of the gas film to generate perturbations with high frequency.

Manuscript received: September 1, 2014 / Revised: February 3, 2015 / Accepted: February 9, 2015

NOMENCLATURE

T = absolute temperature
ρ = air density
μ = air viscosity
p = air pressure
H = bearing clearance
P_s = supply air pressure
R_θ = rotor radius
r = radial distance
R = air constant
ω_θ = rotor angular speed
ω_p = perturbation frequency
p_0 = bearing static air pressure
p_1 = bearing dynamic air pressure
h_0 = bearing static clearance
h_1 = bearing dynamic clearance
θ = angle of the radial direction
V_θ = velocity in the radial direction
U_r = velocity in the tangential direction
p_{tr} = pressure of right thrust bearing
p_{tl} = pressure of left thrust bearing
h_{CT} = air clearance of aerostatic thrust bearing
L_{T1} = length of the aerostatic stator
L_{T2} = distance between right and left thrust bearings
f_P = perturbation frequency

1. Introduction

Due to the high precision, frictionless and no pollution, aerostatic bearings have been widely applied in ultra-precision manufacturing instruments and semiconductor manufacturing equipment.[1-3] Compared with hydrostatic bearings, aerostatic bearings provide low stiffness and low damping because of inherent high compressibility and low viscosity of air. Many studies were mainly focused on characteristics such as the load carrying capacity, stiffness and mass flow rate.[4-8] Particularly, much

attention have been paid to study the pressure depression in the recess,[9,10] which reduces the load carrying capacity of aerostatic bearings.

In the previous study, numerical simulation and experiments carried out by Chen et al.[11,12] have proved that vortices existed in the recess which might cause instabilities of aerostatic bearings. Zhu et al.[13] investigated the transient flow field in the aerostatic bearing using the large eddy simulation method, and further discovered vortex shedding phenomenon in the bearing recess. Computational results demonstrate that vortex shedding causes pressure fluctuation in the bearing clearance, which might cause nano-vibration of aerostatic bearings.

Based on the researches described above, many researchers noted that under certain conditions aerostatic bearings would present complicated dynamic characteristics, such as pressure depression, self-induced oscillation and pneumatic instability. Recently, promoted by requirements of high stability and ultra-precision positioning, more attention has been gradually focused on the dynamic stiffness and stability of aerostatic bearings. Previous studies demonstrated that the dynamic instability of aerostatic bearings was caused by self-excited vibration and pressure depression.[14,15] Bhat et al.[16] studied the performance of inherently compensated flat pad aerostatic bearings subjected to dynamic perturbation forces. They concluded that the pneumatic hammer instability tends to occur at low perturbation frequencies, small orifice diameters, large gap heights and large supply air pressures. Chen et al.[17] studied the effects of recess shapes on the phenomenon of pneumatic hammering in aerostatic bearings, and pointed out that the recess shape significantly affected the vibration status of the pneumatic hammer. The improvement of the dynamic stiffness and stability of aerostatic bearings has become an important topic of research in recent years. Aguirre et al.[18] proposed an active compensation strategy based on air gap shape control with piezoelectric actuators, which can achieve high dynamic stiffness and high bandwidth disturbance compensation. Morosi[19] presented active bearings for high performance turbo machinery and demonstrated the feasibility of applying active lubrication to gas journal bearings.

In summary, the dynamic characteristics of aerostatic bearings have been studied in different approaches, such as CFD simulation,[10,20] numerical methods[6,14,21] and experiments.[12,17,22] However, there are some insufficiencies in dynamic characteristics analysis of aerostatic bearings, especially when they are subjected to dynamic perturbation forces. In this paper, based on the perturbation theory, CFD simulation models are built up to study the dynamic characteristics of the aerostatic bearing using dynamic mesh models method. The main point of this paper is to study the dynamic stiffness and damping coefficients of the aerostatic bearings under various working conditions, when aerostatic bearings are subjected to dynamic perturbation forces.

2. Numerical Method

When aerostatic bearing spindles are subjected to the axial dynamic perturbation forces, their dynamic characteristics are mainly influenced by the performance of the aerostatic thrust bearings rather than aerostatic journal bearings. Therefore, the axial dynamic stiffness and damping coefficients are applied as performance indices to evaluate the dynamic characteristics of aerostatic bearing spindles in this paper.

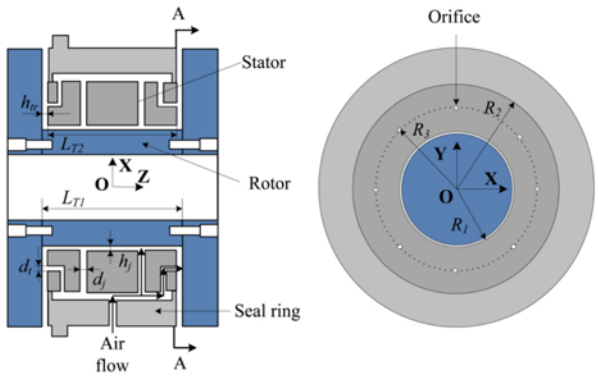

Fig. 1 Bearing configuration: (a) Diagram of aerostatic bearing spindle model and (b) Section A-A

Table 1 Principal parameters of the aerostatic bearing spindle

Symbol	Description	Length (mm)
R_1	inner radius of the aerostatic thrust bearing	25.00
R_2	outer radius of the aerostatic thrust bearing	50.00
R_3	mean radius of the aerostatic thrust bearing	37.50
d_t	orifice radius of the aerostatic thrust bearing	0.20
d_j	orifice radius of the aerostatic journal bearing	0.20
h_j	air clearance of the aerostatic journal bearing	0.03
L_{T2}	length of the aerostatic stator	56.00
L_{T1}	distance between right and left thrust bearing	56.06

2.1 Aerostatic bearing spindle model

For aerostatic bearing spindles, both journal bearings and thrust bearings are required to provide suspension forces and stiffness in radial direction and axial direction. The schematic diagram of the aerostatic bearing spindle with inherently compensated orifice is shown in Fig. 1. This aerostatic bearing spindle includes one aerostatic journal bearing and two aerostatic thrust bearings. Both left and right aerostatic thrust bearing have a single row of 8 identical inherently compensated orifices arranged uniformly at the mean radius. Table 1 shows the principal dimension parameters of the aerostatic bearing spindle in this paper.

2.2 Basic equation

In the cylindrical coordinates system, Reynolds equation for aerostatic bearings is derived as follows[23]

$$\frac{\partial}{\partial r}\left(\frac{\rho h^3}{12\mu}\frac{\partial p}{\partial r}\right)+\frac{1}{r^2}\frac{\partial}{\partial \theta}\left(\frac{\rho h^3}{12\mu}\frac{\partial p}{\partial \theta}\right)=\frac{U_r}{2}\frac{\partial(\rho h)}{\partial r}+\frac{\omega_\theta R_\theta}{2r}\frac{\partial(\rho h)}{\partial \theta}+\frac{\partial(\rho h)}{\partial t} \quad (1)$$

For dynamic characteristics, perturbation should be taken into account. As the clearance height is varied with dynamic perturbation forces, the pressure distribution in air film changes accordingly. The pressure perturbation equation and the clearance height perturbation equation are respectively expressed as follows

$$P = p_0 + p_1 e^{i\omega_p t} \quad (2)$$

$$H = h_0 + h_1 e^{i\omega_p t} \quad (3)$$

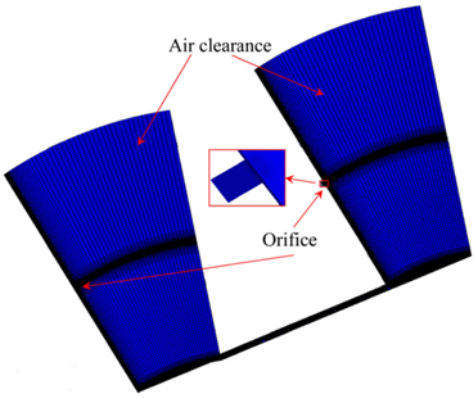

Fig. 2 Computational 3D-model of the aerostatic bearing spindle

Combining the above-mentioned equations, the static equation and perturbation equation based on the perturbation theory are respectively obtained as follows

Static equation:

$$\frac{\partial^2}{\partial r^2}(p_0^2)+\frac{1}{r^2}\frac{\partial^2}{\partial\theta^2}(p_0^2)+\frac{\omega_\theta}{2}\frac{\partial(p_0h_0)}{\partial\theta} \tag{4}$$

Perturbation equation:

$$\frac{h_0^3}{12\mu}\frac{\partial^2}{\partial r^2}p_0p_1+\frac{h_0^3}{12\mu r^2}\frac{\partial^2}{\partial\theta^2}p_0p_1=RT\left(i\omega_p+\frac{\omega_\theta}{2}\right)(p_0h_1+p_1h_0) \tag{5}$$

Then, the load capacity W of aerostatic bearings is calculated by integrating film pressure, as shown in Eq. (6). The axial dynamic load capacity W_d of the aerostatic bearing spindle is calculated using Eq. (7)

$$W=\iint p\,dx\,dy \tag{6}$$

$$W_d=W_r-W_l \tag{7}$$

where, W_r and W_l are calculated by integrating right and left thrust bearing film pressure, respectively.

The pressure distribution in air film varies with displacement perturbation. By using the above equations, the dynamic load capacity can be obtained by integrating the pressure. For the dynamic load capacity, the axial dynamic stiffness K and damping coefficients C can be expressed as follows

$$w_d=-(K+j\omega C) \tag{8}$$

2.3 Numerical simulation

The dynamic characteristics of the aerostatic bearing are studied by using the commercial CFD software ANSYS-Fluent. As shown in Fig. 2, one-sixteenth of 3D computational grid is built up according to the symmetry of the aerostatic bearing spindle. Hexahedral control volumes are employed in the computational domain with satisfactory accuracy. The dynamic mesh model in CFD software is adopted to calculate the time-dependent pressure field. The computational model includes four boundary conditions: solid wall, inflow boundary, outflow boundary and symmetry boundary. The boundary conditions are specified explicitly. The solid walls are assumed to be impermeable and

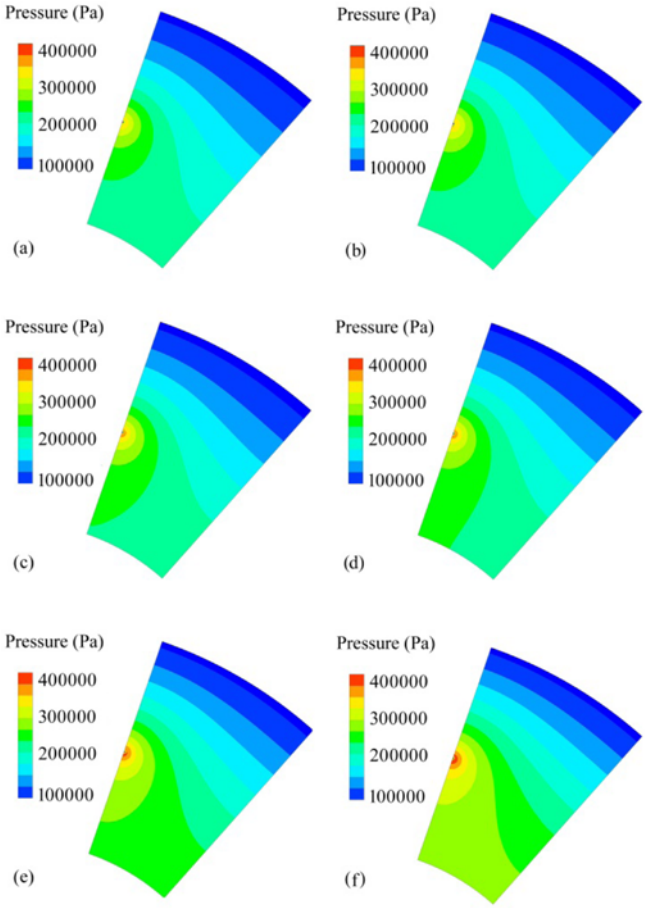

Fig. 3 The pressure distribution of the right film wall at t=3T/4 under perturbations with the same amplitude and different frequencies (a: f_P= 0 Hz; b: f_P=10 Hz; c: f_P=40 Hz; d: f_P=100 Hz; e: f_P=400 Hz; f: f_P=1000 Hz)

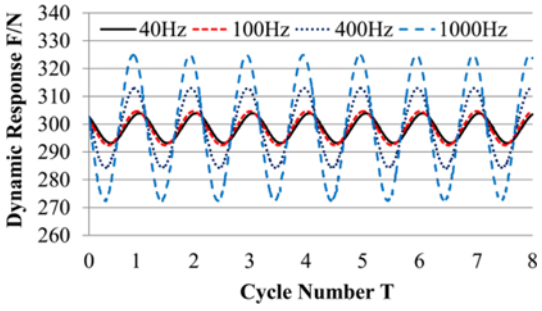

Fig. 4 The Dynamic Responses of the right film wall under different perturbations with the same perturbation amplitude

adiabatic. The walls of the right thrust bearing and left thrust bearing are respectively specified as a sinusoidal motion boundary by user-defined- functions. Mesh motion methods in CFD software are available to update the volume mesh in the deforming regions subjected to the motion defined at the boundaries. To obtain a satisfactory agreement with the utilized experimental data, the turbulence intensities in the inflow and outflow boundaries have been assumed to 7%.[10] In the symmetry plane, the symmetry boundary condition is specified as zero

normal velocity and zero normal gradients of all variables.

The transient pressure distribution of the aerostatic bearing under displacement perturbations with the same amplitude and different frequencies are numerically calculated by using CFD method. As shown in Fig. 3, the pressure distribution of the right film wall at time t=3T/4 for each perturbations are compared. The results show that the pressure distribution remarkably increases as the displacement perturbation frequency increases. This is due to the well-known "squeeze film effects".[24] In another word, when the height of the gas film reduces rapidly, there is not enough time for the corresponding volume of gas to flow out of the gas film.

As shown in Fig.4, the variations of the dynamic force response in eight periods under displacement perturbations with the same amplitude and different frequencies are numerically calculated by using CFD method. The result shows that the force variation remarkably increases as the displacement perturbation frequency increases. Consequently, the dynamic stiffness increase as the perturbation frequency increase.

3. Experiments

To validate the CFD simulation model, the experiment apparatus are fabricated to study the dynamic characteristics of the aerostatic bearing spindle, as shown in Fig. 5. Two aerostatic thrust bearings of the aerostatic bearing spindle are connected to the coil of voice coil motor (Akribis® AVM-90) and dynamic force sensor (Isotron® force sensor 2311-100 with response frequency 75 kHz), respectively. The voice coil motor, whose magnet is mounted on the vibration isolation platform, is used to produce bias current and sinusoidal perturbation force. The guide and slider of the linear motion guide are mounted on the vibration isolation platform and the coil of the motor, respectively. The linear motion guide is used to keep aerostatic bearing spindle axial moving without rotating, because the rotation of the aerostatic bearing spindle has little influence on the dynamic characteristics of the aerostatic bearing spindle under above conditions.

To test the dynamic characteristics of aerostatic bearing spindle, the axial sinusoidal perturbation forces are applied to the stator of the aerostatic bearing spindle. The axial displacement perturbations and the axial dynamic load capacity of the aerostatic bearing spindle are measured by a laser displacement sensor (Keyence® LK-H020 with resolution to 20 nm) and a dynamic force sensor, respectively. The measured data are analyzed by the data acquisition system (LMS® scadas mobile III). Fig. 6 shows the results of the dynamic load capacity and displacement perturbation of the aerostatic bearing spindle subjected to axial dynamic displacement perturbation with five frequencies in 0.1 seconds.

4. Results and Discussion

The dynamic characteristics subjected to the axial dynamic displacement perturbation for the aerostatic bearing spindle are studied by experiments and simulations. The varied factors for each analysis are the perturbation amplitude and frequency, clearance height and supply air pressure.

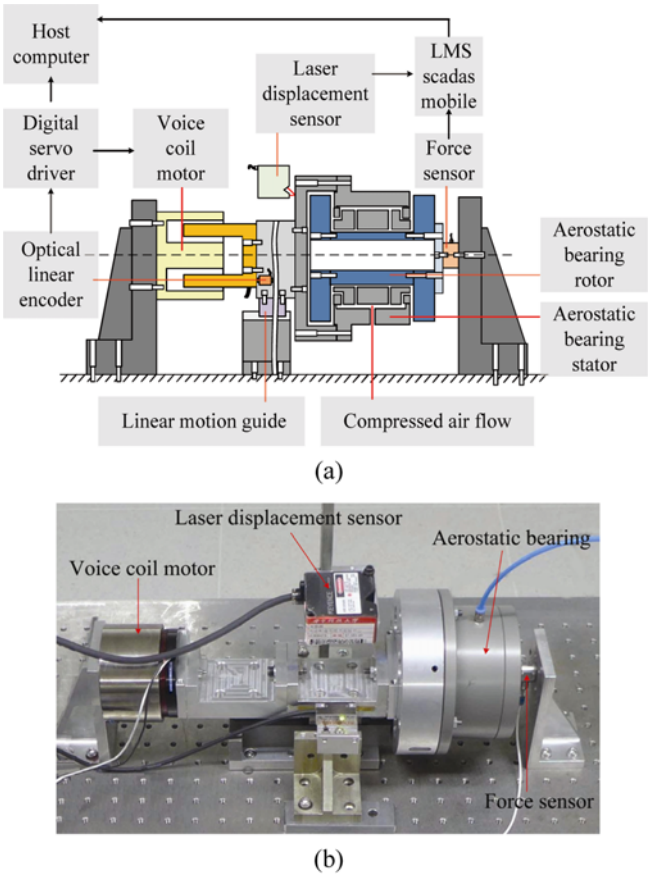

Fig. 5 Experiment setup: (a) Schematic of the test rig, (b) Photo of experiment bench)

4.1 Influence of perturbation amplitude

The varied perturbation amplitudes and frequencies are studied in this analysis, while other factors are constant in order to avoid interference. The analysis results are shown in Figs. 7 and 8. It can be observed that the axial dynamic stiffness and damping coefficients present nonlinear frequency dependence because of air compressibility. The analysis results also show that the axial dynamic stiffness increases as the perturbation frequency increases, while the axial damping coefficient decreases. There is no difference about the axial dynamic stiffness and damping coefficients of the aerostatic bearing spindle subjected to 0.25 μm and 0.5 μm displacement perturbations respectively.

According to the aforementioned simulation and experimental results, the nanoscale amplitudes of axial displacement perturbation have little influence on the stiffness and damping coefficients.

4.2 Influence of supply air pressure

In this analysis, the supply air pressure and the perturbation frequency are varied, while the remaining factors are unchanged. The results from this analysis are shown in Fig. 9 and Fig. 10. The results from this analysis show a similar trend. That is, as the supply air pressure increases, the trend of the axial dynamic stiffness ascends, while the trend of the axial damping coefficient descends. It can be inferred that increasing supply air pressure of aerostatic bearing spindle can achieve higher axial dynamic stiffness and lower axial damping

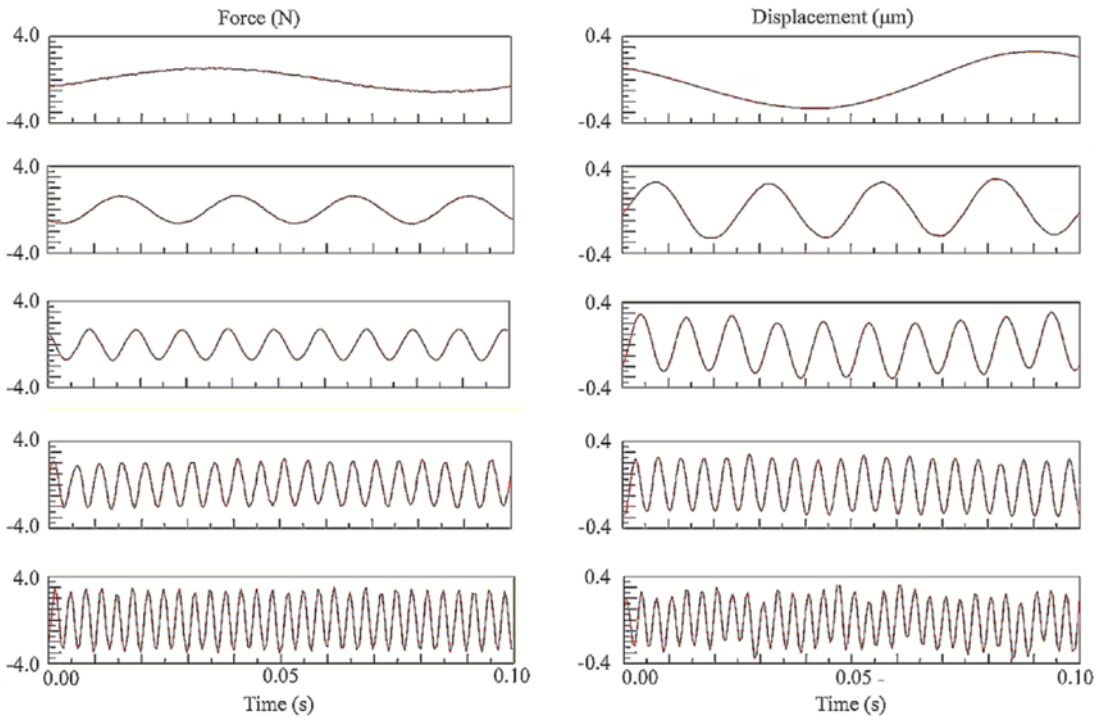

Fig. 6 The results of the dynamic load capacity and displacement perturbations with different frequencies (h_{tr}=25 μm, P_s=0.4 Mpa)

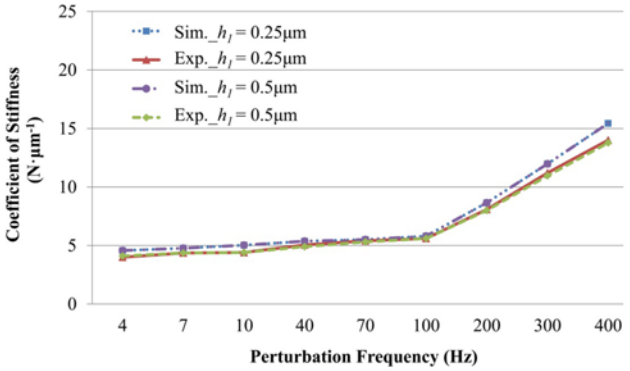

Fig. 7 The axial dynamic stiffness coefficients versus perturbation amplitude (h_{tr}=25 μm, P_s=0.4 Mpa)

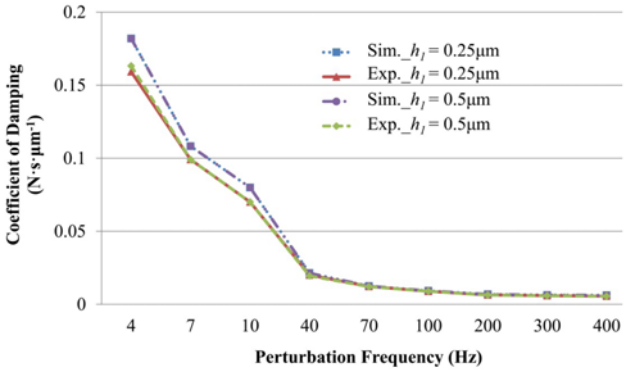

Fig. 8 The axial damping coefficients versus perturbation amplitude (h_{tr}=25 μm, P_s=0.4 Mpa)

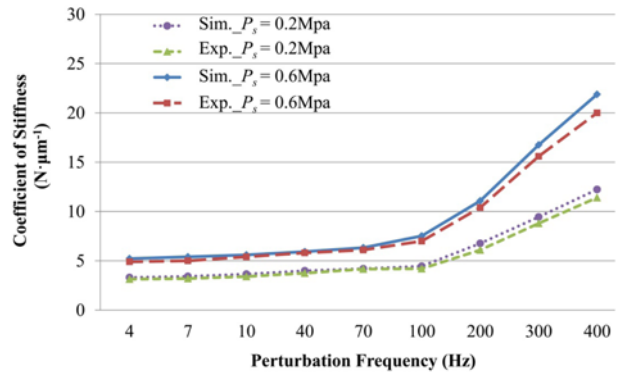

Fig. 9 The axial dynamic stiffness coefficients versus supply air pressure (h_{tr}=25 μm, h_1=0.5 μm)

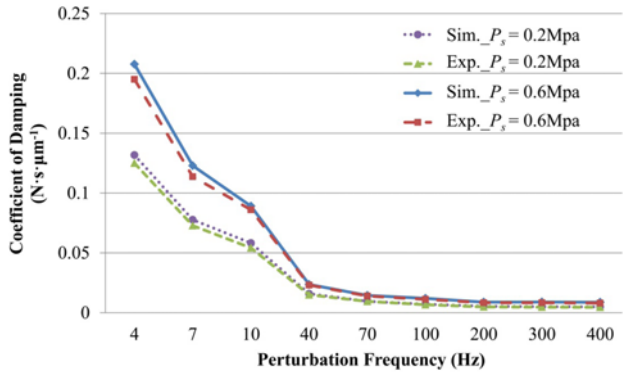

Fig. 10 The axial damping coefficients versus supply air pressure (h_{tr}= 25 μm, h_1=0.5 μm)

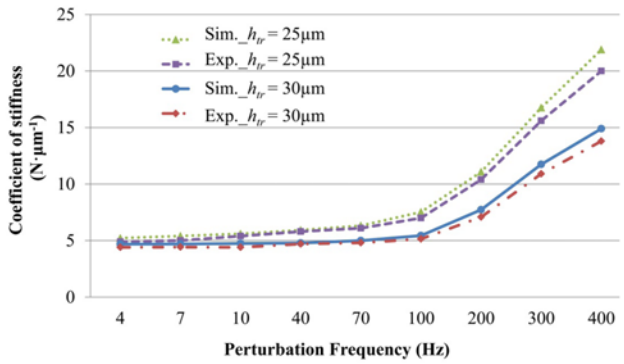

Fig. 11 The axial dynamic stiffness coefficients versus clearance height (P_s=0.6 Mpa, h_1=0.5 μm)

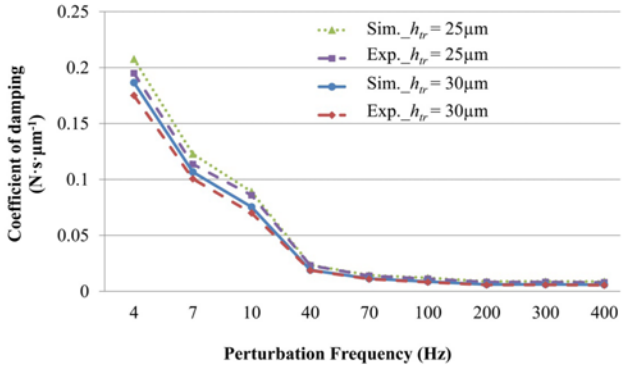

Fig. 12 The axial damping coefficients versus clearance height (P_s=0.6 Mpa, h_1=0.5 μm)

coefficients.

4.3 Influence of clearance height

In this analysis, the varied factors are clearance height and the perturbation frequency. The results from this analysis are plotted in Fig. 11 and Fig. 12. According to the above two figures, it can be observed that as the clearance height increases, the trend of the axial dynamic stiffness descends, while the trend of the axial damping coefficient descends. The results also demonstrate that relatively small the clearance height can achieve higher axial dynamic stiffness and damping coefficients. It is confirmed that the aerostatic bearing spindles with relatively small clearance height can improve dynamic characteristics of aerostatic bearing spindle. Therefore, more attention should be paid to the research on the clearance height in the design of aerostatic bearing spindles.

5. Conclusion and Future Works

The dynamic characteristics subjected to the axial dynamic perturbation forces for the aerostatic bearing spindle with inherently compensated orifice are studied through CFD simulations and experiments. Based on the perturbation theory, a CFD simulation model of the aerostatic bearing spindle is build up to study the dynamic characteristics subjected to the axial dynamic perturbation forces using dynamic mesh models method. The simulation and experiment results demonstrate that the axial dynamic stiffness and damping coefficients are nonlinear frequency dependent because of the air compressibility. In addition, the simulation results are consistent with experiment results well. In conclusion, it was confirmed that the aerostatic bearing spindles with relatively high perturbation frequencies, small clearance heights and high supply air pressures could achieve higher axial dynamic stiffness and lower axial damping coefficients.

Furthermore, the dynamic characteristics subjected to the axial dynamic perturbation forces for aerostatic bearing spindles should be taken into full account in the design of the aerostatic bearing spindle. Active control for dynamic stiffness enhancement will be investigated in the future.

ACKNOWLEDGEMENT

This research was supported by the National Natural Science Foundation of China (No. 51435006, No. 51235005, No. 51405174, and No. 51421062).

REFERENCES

1. Oh, J. S., Khim, G., Oh, J. S., and Park, C. H., "Precision Measurement of Rail Form Error in a Closed Type Hydrostatic Guideway," Int. J. Precis. Eng. Manuf., Vol. 13, No. 10, pp. 1853-1859, 2012.
2. Khim, G., Oh, J. S., and Park, C. H., "Analysis of 5-DOF Motion Errors Influenced by the Guide Rails of an Aerostatic Linear Motion Stage," Int. J. Precis. Eng. Manuf., Vol. 15, No. 2, pp. 283-290, 2014.
3. Ro, S. K. and Park, J. K., "A Compact Ultra-Precision Air Bearing Stage with 3-DOF Planar Motions Using Electromagnetic Motors," Int. J. Precis. Eng. Manuf., Vol. 12, No. 1, pp. 115-119, 2011.
4. Yamada, K., Onishi, N., Sekiya, K., and Yamane, Y., "Permeability Control Method with Laser for Porous Bushings of Aerostatic Bearings," Int. J. Precis. Eng. Manuf., Vol. 14, No. 5, pp. 779-784, 2013.
5. Kassab, S. Z., "Empirical Correlations for the Pressure Depression in Externally Pressurized Gas Bearings," Tribology International, Vol. 30, No. 1, pp. 59-67, 1997.
6. Miyatake, M. and Yoshimoto, S., "Numerical Investigation of Static and Dynamic Characteristics of Aerostatic Thrust Bearings with Small Feed Holes," Tribology International, Vol. 43, No. 8, pp. 1353-1359, 2010.
7. Zhang, Q. and Shan, X., "Dynamic Characteristics of Micro Air Bearings for Microsystems," Microsystem Technologies, Vol. 14, No. 2, pp. 229-234, 2008.
8. Otsu, Y., Miyatake, M., and Yoshimoto, S., "Dynamic Characteristics of Aerostatic Porous Journal Bearings with a Surface-Restricted

Layer," Journal of Tribology, Vol. 133, No. 1, Paper No. 011701, 2011.

9. Kassab, S. Z., "Empirical Correlations for the Pressure Depression in Externally Pressurized Gas Bearings," Tribology International, Vol. 30, No. 1, pp. 59-67, 1997.
10. Eleshaky, M. E., "CFD Investigation of Pressure Depressions in Aerostatic Circular Thrust Bearings," Tribology International, Vol. 42, No. 7, pp. 1108-1117, 2009.
11. Chen, X. D. and He, X. M., "The Effect of the Recess Shape on Performance Analysis of the Gas-Lubricated Bearing in Optical Lithography," Tribology International, Vol. 39, No. 11, pp. 1336-1341, 2006.
12. Chen, X., Chen, H., Luo, X., Ye, Y., Hu, Y., and Xu, J., "Air Vortices and Nano-Vibration of Aerostatic Bearings," Tribology Letters, Vol. 42, No. 2, pp. 179-183, 2011.
13. Zhu, J., Chen, H., and Chen, X., "Large Eddy Simulation of Vortex Shedding and Pressure Fluctuation in Aerostatic Bearings," Journal of Fluids And Structures, Vol. 40, pp. 42-51, 2013.
14. Yoshimoto, S., Yamamoto, M., and Toda, K., "Numerical Calculations of Pressure Distribution in the Bearing Clearance of Circular Aerostatic Thrust Bearings with a Single Air Supply Inlet," Journal of Tribology, Vol. 129, No. 2, pp. 384-390, 2007.
15. Talukder, H. and Stowell, T., "Pneumatic Hammer in an Externally Pressurized Orifice-Compensated Air Journal Bearing," Tribology International, Vol. 36, No. 8, pp. 585-591, 2003.
16. Bhat, N., Kumar, S., Tan, W., Narasimhan, R., and Low, T. C., "Performance of Inherently Compensated Flat Pad Aerostatic Bearings Subject to Dynamic Perturbation Forces," Precision Engineering, Vol. 36, No. 3, pp. 399-407, 2012.
17. Ye, Y., Chen, X., Hu, Y., and Luo, X., "Effects of Recess Shapes on Pneumatic Hammering in Aerostatic Bearings," Proceedings of the Institution of Mechanical Engineers, Part J: Journal of Engineering Tribology, Vol. 224, No. 3, pp. 231-237, 2010.
18. Aguirre, G., Al-Bender, F., and Van Brussel, H., "A Multiphysics Model for Optimizing the Design of Active Aerostatic Thrust Bearings," Precision Engineering, Vol. 34, No. 3, pp. 507-515, 2010.
19. Morosi, S. and Santos, I. F., "Active Lubrication Applied to Radial Gas Journal Bearings. Part 1: Modeling," Tribology International, Vol. 44, No. 12, pp. 1949-1958, 2011.
20. Li, Y. T. and Ding, H., "Influences of the Geometrical Parameters of Aerostatic Thrust Bearing with Pocketed Orifice-Type Restrictor on Its Performance," Tribology International, Vol. 40, No. 7, pp. 1120-1126, 2007.
21. Luong, T. S., Potze, W., Post, J. B., Van Ostayen, R. A. J., and Van Beek, A., "Numerical and Experimental Analysis of Aerostatic Thrust Bearings with Porous Restrictors," Tribology International, Vol. 37, No. 10, pp. 825-832, 2004.
22. Schenk, C., Buschmann, S., Risse, S., Eberhardt, R., and Tünnermann, A., "Comparison between Flat Aerostatic Gas-Bearing Pads with Orifice and Porous Feedings at High-Vacuum Conditions," Precision Engineering, Vol. 32, No. 4, pp. 319-328, 2008.
23. Lo, C. Y., Wang, C. C., and Lee, Y.-H., "Performance Analysis of High-Speed Spindle Aerostatic Bearings," Tribology International, Vol. 38, No. 1, pp. 5-14, 2005.
24. Shou, T., Yoshimoto, S., and Stolarski, T., "Running Performance of an Aerodynamic Journal Bearing with Squeeze Film Effect," International Journal of Mechanical Sciences, Vol. 77, pp. 184-193, 2013.